ATLAS Internal Note
TILE-CAL-NO-
December 19, 1995

Electron Response and e/h Ratio of ATLAS Iron-Scintillator Hadron Prototype Calorimeter with Longitudinal Tile Configuration

J.A. Budagov, Y.A. Kulchitsky,[1]
V.B. Vinogradov
JINR, Dubna, Russia

M. Nessi
CERN, Geneva, Switzerland

A.A. Bogush
Institute of Physics, Academy of Sciences, Minsk, Belarus

V.V. Arkadov
MEPI, Moscow & JINR, Dubna, Russia

G.V. Karapetian
YerPI, Yerevan, Armenia & CERN, Geneva, Switzerland

Abstract

The detailed information about electron response, electron energy resolution and e/h ratio as a function of incident energy E, impact point Z and incidence angle Θ of ATLAS iron-scintillator hadron prototype calorimeter with longitudinal tile configuration is presented. These results are based on electron and pion beams data of $E = 20,\ 50,\ 100,\ 150,\ 300\ GeV$ at $\Theta = 10^o,\ 20^o,\ 30^o$, which were obtained during test beam period in July 1995. The obtained calibration constant is used for muon response converting from pC to GeV. The results are compared with existing experimental data and with some Monte Carlo calculations. For some E, Θ, Z values the local compensation ($e/h = 1$) is observed.

---

[1] *On leave from Institute of Physics, Academy of Sciences, Minsk, Belarus*

1 Introduction

The ATLAS Collaboration proposes to build a general-purpose pp detector which is designed to exploit the full discovery potential of the CERN's Large Hadron Collider (LHC), a super-conducting ring to provide proton – proton collisions around 14 TeV [1]. LHC will open up new physics horizons, probing interactions between proton constituents at the 1 TeV level, where new behavior is expected to reveal key insights into the underlying mechanisms of Nature [2].

The bulk of the hadronic calorimetry in the ATLAS detector is provided by a large (11 m in length, 8.5 m in outer diameter, 2 m in thickness, 10000 readout channels) scintillating tile hadronic barrel calorimeter.

The technology for this calorimeter is based on a sampling technique using steel absorber material and scintillating plates readout by wavelength shifting fibres. An innovative feature of this design is the orientation of the scintillating tiles which are placed in planes perpendicular to the colliding beams staggered in depth [3] (Fig. 1). This geometry combines good performance and a simple and cost effective assembly procedure [4].

In order to test this concept five module prototype of a calorimeter was built and exposed to high energy pion, electron and muon beams at the CERN Super Proton Synchrotron. Results on response, energy resolution and linearity were obtained which confirmed the righteousness of the proposed concept [1], [4], [5].

The aim of this work is to obtain the detailed information about the electron response of this calorimeter and e/h ratios. This information is based on data which were obtained during test beam period in July 1995. Some results about the electron response are obtained in [6] and [7].

2 The Prototype Calorimeter

The prototype calorimeter is composed of five sector modules, each spanning $2\pi/64$ in azimuth, 100 cm in the axial (Z) direction, 180 cm in the radial direction (about 9 interaction lengths), and with a front face of 100×20 cm^2 [5]. The iron structure of each module consists of 57 repeated "periods". Each period is 18 mm thick and consists of four layers (Fig. 2). The first and third layers are formed by large trapezoidal steel plates (master plates), 5 mm thick and spanning the full radial dimension of the module. In the second and fourth layers, smaller trapezoidal steel plates (spacer plates) and scintillator tiles alternate along the radial direction. The spacer plates are 4 mm thick and of 11 different sizes. Scintillator tiles are 3 mm thickness. The iron to scintillator ratio is 4.67:1 by volume.

Radially oriented WLS fibres collect light from the tiles at both of their open edges and bring it to photo-multipliers (PMTs) at the periphery of the calorimeter. Each PMT views a specific group of tiles, through the corresponding bundle of fibres. With this readout scheme three-dimensional segmentation is immediately obtained.

Tiles of 18 different shapes all have the same radial dimensions (10 cm). The prototype calorimeter is radially segmented into four depth segments by grouping fibres from different tiles. Proceeding outward in radius, the three smallest tiles, $1 \div 3$ are grouped into section 1, $4 \div 7$ into section 2, $8 \div 12$ into section 3 and $13 \div 18$ into section 4. The readout cell width in Z direction is about 20 cm.

3 Test Beam Layout

The five modules have been positioned on a scanning table, able to allow high precision movements along any direction. Upstream of the calorimeter, a trigger counter telescope was installed, defining a beam spot of 2 cm diameter. Two delay-line wire chambers, each with Z, Y readout, allowed to reconstruct the impact point of beam particles on the calorimeter face to better than $\pm$ 1 mm [4]. A helium Čerenkov threshold counter was used to tag π-mesons and electrons for $E = 20\ GeV$. A large scintillator wall covering about 1 m^2 of surface has been placed on the side and on the back of the calorimeter to quantify back and side leakage.

4 Data Taking and Event Selection

Data were taken with electron and pion beam of 20, 50, 100, 150, 300 GeV at $\Theta = 10^o, 20^o, 30^o$ and $Z = -8 \div -36$ cm. Number of runs about 60, number of events is approximately a half of million. The treatment was carried out using program TILEMON [8].

As a result we have for each event 200 values of charges Q_{ijkl} from PMT properly calibrated [5] with pedestal subtracted. Here indexes i, j, k, l mean: $i = 1, \ldots, 5$ is the raw number, $j = 1, \ldots, 5$ is the module number, $k = 1, \ldots, 4$ is the depth number and $l = 1, 2$ is the PMT number.

The Table 1 represents the volume of analyzed information. To separate electrons from pions the following criteria were proposed which are given in Table 2. The cuts 1 and 2 remove beam halo. The cut 3 removes muons and nonsingle-track events. The cuts 4 and 5 carry out electron-pion separation (Fig. 3 $\div$ Fig. 7). The cut 4 is connected with Čerenkov counter amplitude (S_{Cer}). Cut 5 is the relative shower energy deposition in the first two calorimeter depths, where the indexes i and k in Q_{ijkl} determine the regions of electromagnetic shower development and

$$C_i = \sum_{selected\ i} \sum_{j=3} \sum_{k=1}^{2} \sum_{l=1}^{2} Q_{ijkl}/E, \tag{1}$$

$$E = \sum_{ijkl} Q_{ijkl}. \tag{2}$$

The values C_i depend on a particle's entry angle Θ.

The basis for electron-hadron separation is the different longitudinal energy deposition for electrons and hadrons. A particle traversing the first two calorimeter depths at $10^o \div 30^o$ angles crosses $55 \div 63$ cm of iron. It corresponds to $31 \div 36$ radiation length or $3.3 \div 3.8$ nuclear interaction ones. The amount of energy deposited is equal to approximately 100% for the electromagnetic shower and about half for hadronic one [9].

Fig. 3 shows the distribution of electron and pion events as a function of E and the value of Čerenkov counter signal. Two group of events are observed.

Figures 4 $\div$ 6 show the distribution of the electron and pion events for $E = 20\ GeV$ at $\Theta = 10^o$ as a function of C_i for electrons (Fig. 4) and for pions (Fig. 5) tagged by Čerenkov counter and for all events (Fig. 6).

The values σ for each energy were obtained by Gaussian fit of spectra region around 1 where pronounced peaks are observed (Fig. 7).

From these Figures some estimations of pion and electron contaminations were obtained. At 20 GeV electron contamination in pion region does not exceed the 3% level and pion contamination in the electron region is less 6%. These contaminations considerably decrease with energy increasing.

Fig. 7 shows the distribution of all events as a function of C_i for $E = 300\ GeV$ at $\Theta = 30^o$. At this energy pion contamination in electron region does not exceed the 1% level.

5 Results

5.1 Electrons

5.1.1 Response

As to electron response our calorimeter is very complicated object. It may be imagined as a continuous set of calorimeters with the variable absorber and scintillator thicknesses (from $t = 81$ to 28 mm and from $s = 17$ to 6 mm for $10^o \leq \Theta \leq 30^o$), where t and s are the thicknesses of absorber and scintillator respectively.

Therefore an electron response ($R = E/E_{beam}$) is rather complicated function of E_{beam}, Θ and Z. Energy spectrum for given run (beam has the transversal spread $\pm 10\ mm$) is non-Gaussian (Fig. 8), but it becomes Gaussian for given E, Θ, Z values.

The normalized electron response for $E = 20\ GeV$ at $\Theta = 10^o$ is shown in Fig. 9 as a function of impact point Z coordinate. One can see the clear periodical structure of the response with 18 mm period.

The mean over two 18 mm periods responses R and relative spreads ($\Delta R/R = (R_{max} - R_{min})/R_{mean}$) as a function of E and Θ are presented in Table 3. The relative spread decreases with energy increasing from 16% at $E = 20\ GeV$, $\Theta = 10^o$ to 4% at $E = 300\ GeV$, $\Theta = 30^o$. For $\Theta = 10^o$ the significant relative spread decreasing with energy increasing is observed. For $\Theta = 20^o$ and 30^o spreads decrease more slowly. In all energies the spread decreasing with the angle increasing is observed. The mean value R for all angles and energies is $5.69 \pm 0.04\ (stat.)\ \pm 0.15\ (syst.)\ pC/GeV$. As a systematic error the estimate of r.m.s. of distribution of values R is used. In [10] the experimental data on muon response have been converted from pC to GeV using this calibration constant.

We attempted to explain the electron response as a function of Z coordinate calculating the total number of shower electrons (positrons) crossing scintillator tiles using the shower curve (the number of particles in the shower N_e as a function of the longitudinal shower development) which is given in [11]. These calculations were performed for all energies and angles for trajectories entering into four different elements of calorimeter periodic structure — spacer, master, tile, master (Fig. 2). The results for $E = 20\ GeV$ at $\Theta = 10^o$ normalized and attached to the experimental response at $Z = -88.5\ mm$ (Fig. 9) are given in Table 4 together with the experimental data. Such simple calculations are in agreement with data at $E = 20\ GeV$ but do not reproduce spread decreasing with energy increasing. The latter is connect with increasing the shower lateral spread with energy increasing.

5.1.2 Energy Resolution

For all analyzed electron data the energy resolutions for different values E, Θ, Z were obtained. As an example, Fig. 10 shows the energy resolution as a function of Z for $E = 20\ GeV$ at $\Theta = 10^o$. Data reveal some structures in the Z dependence but with smaller spread than the response one. The energy resolutions averaged over two 18 mm Z period are shown in Fig. 11 as a function of $1/\sqrt{E}$ and presented in Table 5. The calculations of energy resolution values were performed without restricting on the area around the peak value.

Fits of these data by the formulae

$$\frac{\sigma}{E} = \frac{a}{\sqrt{E}} + b, \tag{3}$$

$$\frac{\sigma}{E} = \frac{a}{\sqrt{E}} \oplus b, \tag{4}$$

are given in Table 6. These two expressions describe the data satisfactorily. The values of statistical term a about the same for these cases, and the values of constant term b about three times is greater in quadratic summing (4). The statistical term a of the resolution decreases from $\approx$ 65% (for 10^o) to $\approx$ 35% (for 30^o).

The energy resolution of the 10^o data is significantly worse than for 20^o and 30^o ones. Consideration of the 10^o trajectories traversing the calorimeter showed that in this case on the way of shower the large iron ununirformities exist. For example, for the trajectory entering in to the master plate the next structure

$$81\ Fe - Sc - 29\ Fe - Sc - 132\ Fe - Sc - 23\ Fe - Sc - 29\ Fe - Sc - 81\ Fe - Sc \tag{5}$$

is observed (thickness of Fe in mm, thickness of scintillator Sc is equal to 17 mm). At the same time due to the relatively short electromagnetic shower length only few scintillator tiles effectively works. For example, at 20 GeV 80% shower particles cross only two tiles. All this result in large energy deposition fluctuations.

From some point of view, our calorimeter may be considered as a calorimeter with variable sampling steps (5). In [12] the optimization of electromagnetic calorimeter at variable sampling steps have been studied. It was shown, that optimization of the sampling layers (samplers) positions give significantly better energy resolution with compare to a conventional, constant sampling one. In our case, probably, on the contrary positions of samplers have not lead to the electron energy resolution improvement. It is to be noted that it concerns only the energy resolution for electrons but for this the calorimeter was not designed.

We compared our results on energy resolution with parametrization from [13]:

$$\frac{\sigma}{E} = \frac{a}{\sqrt{E}} = \frac{\sigma_o}{\sqrt{E}} \cdot \left(\frac{t}{X_t}\right)^{\gamma} \cdot \left(\frac{s}{X_s}\right)^{\delta}, \tag{6}$$

where $\sigma_o = 6.33\ \% \cdot \sqrt{GeV}$, $\gamma = 0.62$, $\delta = 0.21$ are the parameters, X_t and X_s are the radiation lengths of iron and scintillator respectively. In our case the values of t and s are equal to: $t = 14\ mm/\sin\Theta$, $s = 3\ mm/\sin\Theta$. This formula is purely empirical and the parameters σ_o, γ, δ were determined by fitting Monte Carlo data.

The results of calculations are given in Table 7. As can be seen from this Table the energy resolutions calculated by formula (6) are more accurate than experimental ones but it is necessary to note that there is the non-adequateness of our calorimeter in comparison with Monte Carlo calculations (non-uniformity along direction of the shower development, non normal incidence). Besides, the given in [13] values of σ_o, γ, δ are not quite adequate for our 10^o and 20^o because these parameters were determined for the iron – scintillator with $s \leq 10$ mm and $t \leq 35$ mm.

5.2 Pion Response

The energy spectra for all studied energies and angles were obtained. As an example, the observed energy spectrum for 20 GeV at 20^o is shown in Fig. 12. The spectrum displays small or no tails. Above 150 GeV some low energy tail appears due to longitudinal leakage of the hadronic shower.

Pion data don't reveal any structure (Fig. 13) with the exception of data at $E = 300\ GeV$. This ununiformity was noted previously by M. Bosman [14]. This effect may be related with the energy leakage.

5.3 e/h Ratio

The responses obtained for e and π give the possibility to extract e/h value, the ratio of the calorimeter responses to the electromagnetic (e) and non-electromagnetic (purely hadronic) components of hadron showers. As it is known the value $e/h \neq 1$ causes deviation from linearity in the hadronic response versus energy, besides broadening the energy resolution [16]. The value of the e/h ratio as shown in [15] depends on a big number of factors, among them, the thickness of the passive layers, the thickness of the active layers, the sampling fraction. The e/h ratio of a sampling calorimeter with an iron – scintillator ratio less than 20 is expected [16] to be > 1 for the conventional orientation of tiles with respect to incident hadrons.

In our case the electron – pion ratios reveal complicated structures $e/\pi = f(E, \Theta, Z)$. As an example, Fig. 14 shows e/π ratio as a function of Z coordinate for $E = 20\ GeV$ at $\Theta = 10^o$.

For some Z points the local compensation (the equalization of the electromagnetic and hadronic signals, $e/\pi = e/h = 1$) is observed. This is the first experimental observation of compensation in iron-scintillator calorimeters. Compensation in these calorimeters had been predicted in [16] but in considerably greater value of $R_d = t/s$ (much more 10) than our $R_d = 4.7$ value. Reconsideration has led Wigmans ([16]) to the conclusion that for thick absorber plates e/h value depends also on the plates thickness and not only on R_d and e/h is predicted to become 1 for plates of ≈ 110 mm. In our case the iron thickness is equal to ≈ 80 mm.

The e/π ratios averaged over two 18 mm period, are given in Table 8 and shown in Fig. 15 as a function of beam energy.

The e/h ratios were extracted from these data by the formula [15]:

$$e/\pi = \frac{e/h}{1 + (e/h - 1) \cdot 0.11 \cdot lnE}. \tag{7}$$

Fitted e/h values are given in Table 9 with the other existing experimental data for iron-scintillator calorimeters together with the corresponding values of thickness of the iron absorber (t), thickness of the readout scintillator layers (s) and the ratio $R_d = t/s$ (Fig. 16).

The e/h values generally decrease with increasing of iron thickness (Fig. 17). Besides, some data, [18] and [21], fall out from the general picture. The result of [18] may be discarded because in this work as the authors have written the e/π signal ratio is roughly estimated and only at 25 GeV.

At the same time the considerable disagreement between different Monte Carlo calculations [16], [23] and experimental data is observed.

Accordingly [16] the reason of e/h decrease is because the hadron signal (h) increases owing to more neutrons released in hadronic shower with iron thickness increasing while electron signal (e) decreases owing to more absorption of the electromagnetic shower.

Fig.18 shows the e/h ratios as a function of scintillator thickness. We observe a decreasing e/h value in comparison with increasing scintillator thickness. Besides, it is seen that the extrapolation of our results and data from [4], [20] by smooth curve is compatible with Monte Carlo calculations [23]. As can be seen from Fig. 17 and 18 there is the clear correlation between the e/h decreasing and the simultaneous t and s thicknesses increasing. This is the first experimental observation of such e/h behavior.

6 Conclusions

We have investigated the various properties of hadron tile calorimeter with respect to electrons. The detailed information about response, energy resolution, e/π-ratio as a functions of incident energy, impact point and angle is obtained.

Some results are following:

- The significant variation of electron response ($3 \div 16$ %) as a function of Z coordinate with 18 mm periodic dependence is observed. The mean value of electron response for all energies and angles is $R = 5.69 \pm 0.04 \ \pm 0.15 \ pC/GeV$.
- The energy resolution data are well fitted by formulae (3) and (4). The statistical term a of the resolution decreases from ≈ 65 % (for 10^o) to ≈ 35 % (for 30^o). The constant term b is in the range of $1 \div 3$ %.
- The e/π-ratios reveal the periodic variation as a function of Z coordinate with spreads $4 \div 13$ %.
- For some E, Θ, Z values the local compensation ($e/h = 1$) is observed.
- Extracted e/h values show the general decreasing tendency for iron and scintillator thicknesses increasing.
- Our results for e/h-ratio are compatible with Monte Carlo calculations of [23] and in disagreement with [16].

7 Acknowledgements

This work is the result of the efforts of many people from ATLAS Collaboration. The authors are greatly indebted to all Collaboration for their test beam setup and data taking.

Authors are grateful Peter Jenni and Nikolai Russakovich for their attention and support of this work. We are thankful Ana Henriques for her support of this analysis and constructive advices on the improvement of paper context. We are indebted to M. Bosman and M. Cavalli-Sforza for the valuable discussions. We are also thankful to I. Efthymiopoulos and I. Chirikov-Zorin for the careful reading and constructive advices on the improvement of paper context.

References

[1] ATLAS Collaboration, CERN/LHCC/94-93, ATLAS Technical Proposal for a General-Purpose pp experiment at the Large Hadron Collider CERN, CERN, Geneva, Switzerland.

[2] LHC News, $N^{\underline{o}}$ 7 September 1995, CERN, Geneva, Switzerland.

[3] O. Gildemeister, F. Nessi-Tedaldi and M. Nessi, Proc. 2nd Int. Conf. on Cal. in HEP, Capri, 1991.

[4] F. Ariztizabal et al., NIM A349 (1994) 384.

[5] E. Berger et al. CERN/LHCC 95-44, Construction and Performance of an Iron-Scintillator Hadron Calorimeter with Longitudinal Tile Configuration, CERN, Geneva, Switzerland.

[6] A. Amorim, M. David, ATLAS TILECAL-TR-24, November 1994, CERN, Geneva, Switzerland.

[7] M. Cavalli-Sforza, M. Pilar Casado, ATLAS TILECAL-TR-43, September 1995, CERN, Geneva, Switzerland.

[8] I. Efthymiopoulos, A. Solodkov, The TILECAL Program for Test Beam Data Analysis, User Manual, 1995, CERN, Geneva, Switzerland.

[9] U. Amaldi, Phys. Scripta 23 (1981) 409.

[10] A. Henriques, G. Karapetian, A. Solodkov, ATLAS Internal Note, TILECAL-No-68, November 1995, CERN, Geneva, Switzerland.

[11] G. Abshire et al., NIM 164 (1979) 67.

[12] A. Prabhaharan and L. Bugge, NIM A314 (1992) 21.

[13] J. Del Peso, E. Ros, NIM A276 (1989) 456.

[14] M. Bosman, ATLAS TILECAL-TR-43, September 1995, CERN, Geneva, Switzerland.

[15] R. Wigmans, NIM A265 (1988) 273.

[16] R. Wigmans, NIM A259 (1987) 389.

[17] S. L. Stone et al., NIM 151 (1978) 387.

[18] Y. A. Antipov et al., NIM 180 (1990) 81.

[19] H. Abramowicz et al., NIM 180 (1981) 429.

[20] V. Bohmer et al., NIM 122 (1974) 313.

[21] M. Holder et al., NIM 151 (1978) 69.

[22] M. De Vincenze et al., NIM A243 (1986) 348.

[23] T. A. Gabriel et al., NIM A295 (1994) 336.

List of Tables

1 The number of analyzed electron and pion runs as a function of incident energy, Θ and Z coordinate of impact on the calorimeter face. 10
2 Cuts for electron events selection. 11
3 The mean relative electron responses R and corresponding spreads ΔR as a function of energy and angle. 11
4 Comparison of measured and calculated electron responses for $E = 20\ GeV$ at 10^o. 11
5 The energy resolution as a function of energy and incidence angles. 12
6 The values of the parameters a and b in the parametrization of the energy resolution. 12
7 The values of parameter a for existing experimental data for iron-scintillator calorimeters. 12
8 The mean e/π ratios and the corresponding spreads as a function of the incidence energy and angle. 13
9 The e/h ratios. 13

List of Figures

1 Principal of the tile hadronic calorimeter. 14
2 Exploded view of an assembled tile calorimeter period. 15
3 Distribution of the events for $E = 20\ GeV$, $\Theta = 10^o$ as a function of values E_{tot} and Čerenkov counter signal. 16
4 Distribution of the events for $E = 20\ GeV$, $\Theta = 10^o$ as a function of C_i for electrons tagged by Čerenkov counter. 17
5 Distribution of the events for $E = 20\ GeV$, $\Theta = 10^o$ as a function of C_i for π- mesons tagged by Čerenkov counter. 18
6 Distribution of the events for $E = 20\ GeV$, $\Theta = 10^o$ as a function of C_i for all events. 19
7 Distribution of the events for $E = 300\ GeV$ electron at $\Theta = 30^o$ as a function of C_i for all events. 20
8 Energy distribution for 20 GeV electrons at 10^o as a function of Z coordinate. . . . 21
9 Response to 20 GeV electrons at 10^o as a function of Z coordinate. 22
10 Energy resolution for 20 GeV electrons at 10^o as a function of Z coordinate. 23
11 Energy resolution for electrons at 10^o, 20^o and 30^o. 24
12 Energy response for 20 GeV pions at 20^o. 25
13 Pion response for 20 GeV and 10^o as a function of Z coordinate. 26
14 The e/π ratio for 20 GeV at 10^o as a function of Z coordinate. 27
15 The e/π ratio as a function of energy at 10^o, 20^o and 30^o. 28
16 The e/h-ratios as a function of iron and scintillator thicknesses ratio. The lines are the results of fits to some selected data. The meaning of symbols see in Table 9. . . 29
17 The e/h-ratios as a function of iron thickness. The lines are the results of fits to some selected data. The meaning of symbols see in Table 9. 30
18 The e/h-ratios as a function of scintillator thickness. The lines is the results of fits to some selected data. The meaning of symbols see in Table 9. 31

Table 1: The number of analyzed electron and pion runs as a function of incident energy, Θ and Z coordinate of impact on the calorimeter face.

Energy (GeV)	Θ^o	Z (cm)	Number of e Runs	Number of π Runs
20	10	- 8 ÷ - 6	2	2
	20	- 20 ÷ - 18	2	2
	30	- 38 ÷ - 36	3	2
50	10	- 8 ÷ - 6	2	2
	20	- 20 ÷ - 18	2	2
	30	- 38 ÷ - 36	2	-
100	10	- 8 ÷ - 6	3	2
	20	- 20 ÷ - 18	2	2
	30	- 38 ÷ - 36	3	-
150	10	- 8 ÷ - 6	2	2
	20	- 20 ÷ - 18	3	-
	30	- 38 ÷ - 36	3	2
300	10	- 8 ÷ - 6	4	2
	20	- 20 ÷ - 18	2	2
	30	- 38 ÷ - 36	3	1

Table 2: Cuts for electron events selection.

Cut		min	max
1	Z^{imp}_{beam}	$-14\ mm$	$8\ mm$
2	Y^{imp}_{beam}	$-15\ mm$	$10\ mm$
3	E_{tot}	E^{min}_{tot}	E^{max}_{tot}
Cut			min
4	$E = 20\ GeV$ & S_{Cer}		180
5	$E \geq 50\ GeV$ & $\Theta = 10^o$, $C_i, i = 3$		$1 - 2 \cdot \sigma$
	$E \geq 50\ GeV$ & $\Theta = 20^o$, $C_i, i = 2, 3$		$1 - 2 \cdot \sigma$
	$E \geq 50\ GeV$ & $\Theta = 30^o$, $C_i, i = 1, 2$		$1 - 2 \cdot \sigma$

Table 3: The mean relative electron responses R and corresponding spreads ΔR as a function of energy and angle.

$R = E/E_{beam}$, (pC/GeV)			
E_{beam}, $GeV \setminus \Theta^o$	10^o	20^o	30^o
20	5.64±0.09	5.68±0.03	5.79±0.03
50	5.42±0.06	5.75±0.03	5.90±0.03
100	5.52±0.05	5.77±0.02	5.85±0.02
150	5.40±0.02	5.67±0.02	5.73±0.02
300	5.78±0.04	5.72±0.02	5.90±0.02
$< R_\Theta >$	5.53±0.05	5.72±0.06	5.83±0.05
$< \Delta R_\Theta >$	±0.15 (2.8%)	±0.16 (2.8%)	±0.11 (1.9%)
$< R >$	5.69±0.04±0.15		

Spreads ΔR, $(\Delta R/R)$			
20	±0.9 (16.0%)	±0.30 (9.4%)	±0.25 (4.3%)
50	±0.7 (12.9%)	±0.25 (4.4%)	±0.20 (3.4%)
100	±0.6 (10.9%)	±0.25 (4.4%)	±0.20 (3.4%)
150	±0.3 (5.6%)	±0.25 (4.4%)	±0.15 (2.6%)
300	±0.35 (6.3%)	±0.20 (3.7%)	±0.20 (3.5%)

Table 4: Comparison of measured and calculated electron responses for $E = 20\ GeV$ at 10^o.

Z, mm	Element	Total N_e	R, (pC/GeV)	
			calcul.	exper.
−88.5	spacer	384	6.5	6.5
−84.0	master	333	5.6	5.7
−79.5	tile	291	4.9	4.9
−75.0	master	354	5.9	5.8

Table 5: The energy resolution as a function of energy and incidence angles.

E, $GeV \setminus \Theta^o$	10^o	20^o	30^o
20	14.86±0.11	9.32±0.15	8.89±0.13
50	9.38±0.13	5.85±0.10	4.43±0.07
100	6.94±0.14	3.85±0.05	3.36±0.06
150	5.90±0.15	4.16±0.15	2.21±0.17
300	4.96±0.13	2.92±0.10	2.44±0.05

Table 6: The values of the parameters a and b in the parametrization of the energy resolution.

	$\sigma/E = a/\sqrt{E} + b$		$\sigma/E = a/\sqrt{E} \oplus b$	
Θ^o	a (%)	b (%)	a (%)	b (%)
10	61.1±1.8	1.0±0.3	64.6±0.7	2.9±0.2
20	38.6±3.0	0.3±0.3	39.1±2.6	1.3±0.9
30	33.4±4.9	0.2±0.5	33.7±1.1	1.1±1.1

Table 7: The values of parameter a for existing experimental data for iron-scintillator calorimeters.

Author	Ref.	t	s	a	a_{calc}
Stone	[17]	4.8	6.3	10.	7.0
Antipov	[18]	20.	5.0	27.	17.
Abramovicz	[19]	25.	5.0	23.	20.
our data 30^o		28.	6.0	34. ± 1.	20.
our data 20^o		41.	9.0	39. ± 3.	24.
our data 10^o		81.	17.	65. ± 1.	32.

Table 8: The mean e/π ratios and the corresponding spreads as a function of the incidence energy and angle.

e/π ratio			
E, $GeV \setminus \Theta^o$	10^o	20^o	30^o
20	1.148±0.017	1.178±0.006	1.197±0.004
50	1.096±0.012	1.172±0.005	1.198±0.006
100	1.102±0.009	1.155±0.004	1.182±0.005
150	1.083±0.008	1.141±0.005	1.165±0.004
300	1.088±0.006	1.106±0.004	1.149±0.005
Spreads for e/π ratio			
20	±0.15 (13.1%)	±0.063 (5.4%)	±0.055 (4.6%)
50	±0.14 (12.8%)	±0.050 (4.3%)	±0.065 (5.4%)
100	±0.11 (10.0%)	±0.050 (4.3%)	±0.055 (4.7%)
150	±0.063 (5.8%)	±0.080 (7.1%)	±0.060 (5.2%)
300	±0.075 (7.2%)	±0.038 (3.5%)	±0.050 (4.5%)

Table 9: The e/h ratios.

Author	Ref.	R_d	t, mm	s, mm	e/h	Symbols
Bohmer	[20]	2.8	20.	7.0	1.44	●
Wigmans	[16] *	3.0	15.	5.0	1.25	▲
Antipov	[18]	4.0	20.	5.0	1.15	○
Wigmans	[16] *	4.0	20.	5.0	1.23	▲
TileCal, 30°		4.7	28.	6.0	1.39 ± 0.03	■
TileCal, 20°	[4]	4.7	41.	9.0	1.37 ± 0.02	□
TileCal, 20°		4.7	41.	9.0	1.34 ± 0.03	■
TileCal, 10°		4.7	81.	17.	1.23 ± 0.02	■
Wigmans	[16] *	5.0	25.	5.0	1.21	▲
Abramovicz	[19]	5.0	25.	5.0	1.32	◊
Vincenzi	[22]	5.0	25.	5.0	1.32	★
Wigmans	[16] *	6.0	30.	5.0	1.20	▲
Gabriel	[23] *	6.3	19.	3.0	1.55	▼
Wigmans	[16] *	8.0	40.	5.0	1.18	▲
Holder	[21]	8.3	50.	6.0	1.18	∗
Gabriel	[23] *	8.5	25.4	3.0	1.50	▼
Wigmans	[16] *	10.	50.	5.0	1.16	▲

---

* Monte Carlo calculations

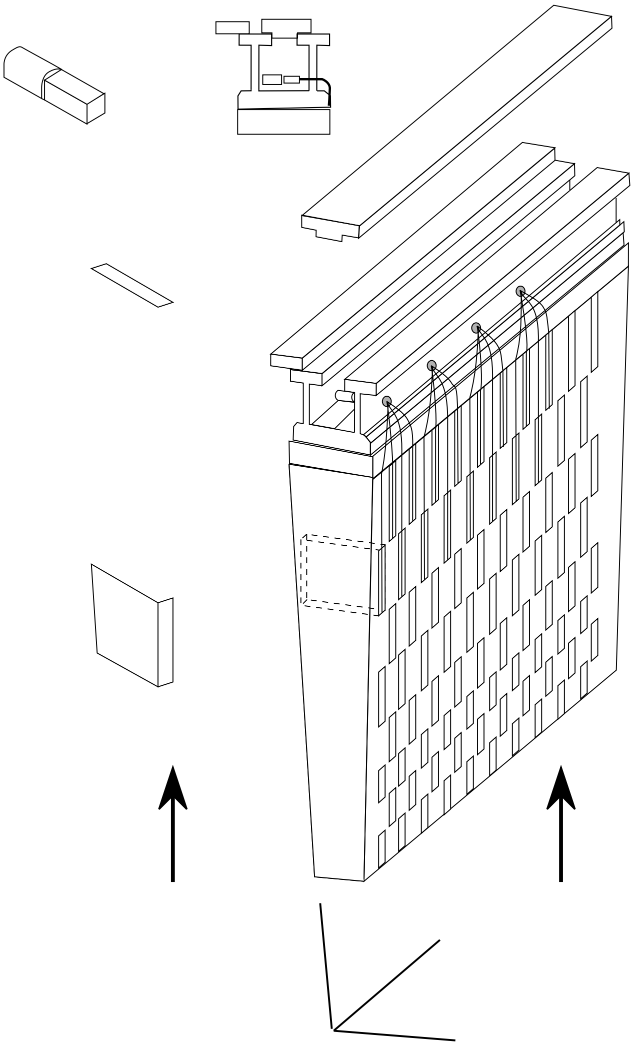

Figure 1: Principal of the tile hadronic calorimeter.

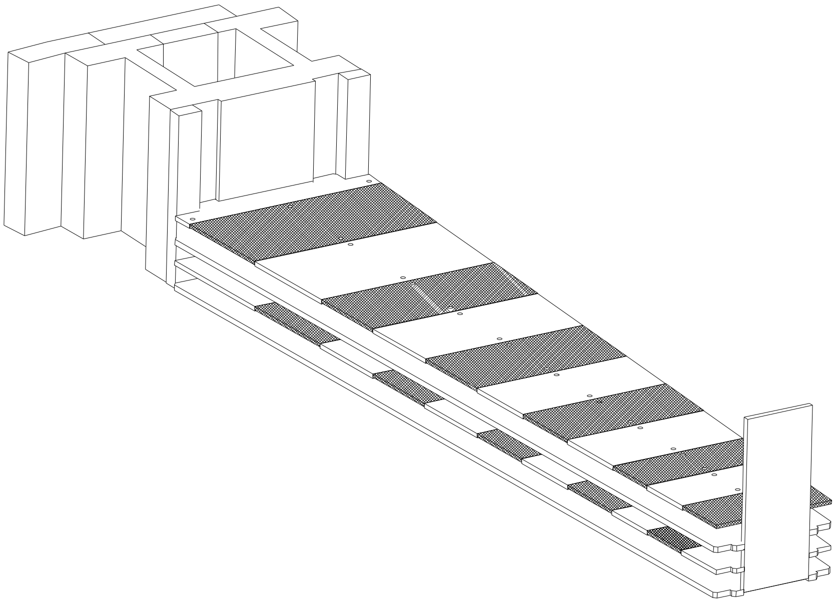

Figure 2: Exploded view of an assembled tile calorimeter period.

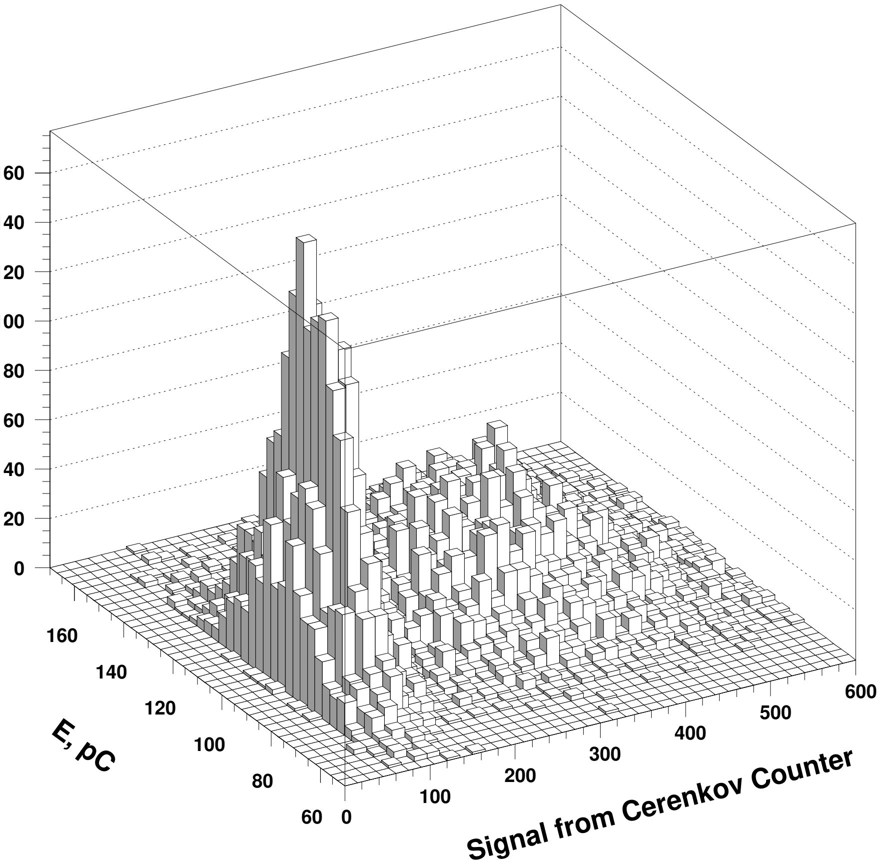

Figure 3: Distribution of the events for $E = 20\ GeV$, $\Theta = 10^o$ as a function of values E_{tot} and Čerenkov counter signal.

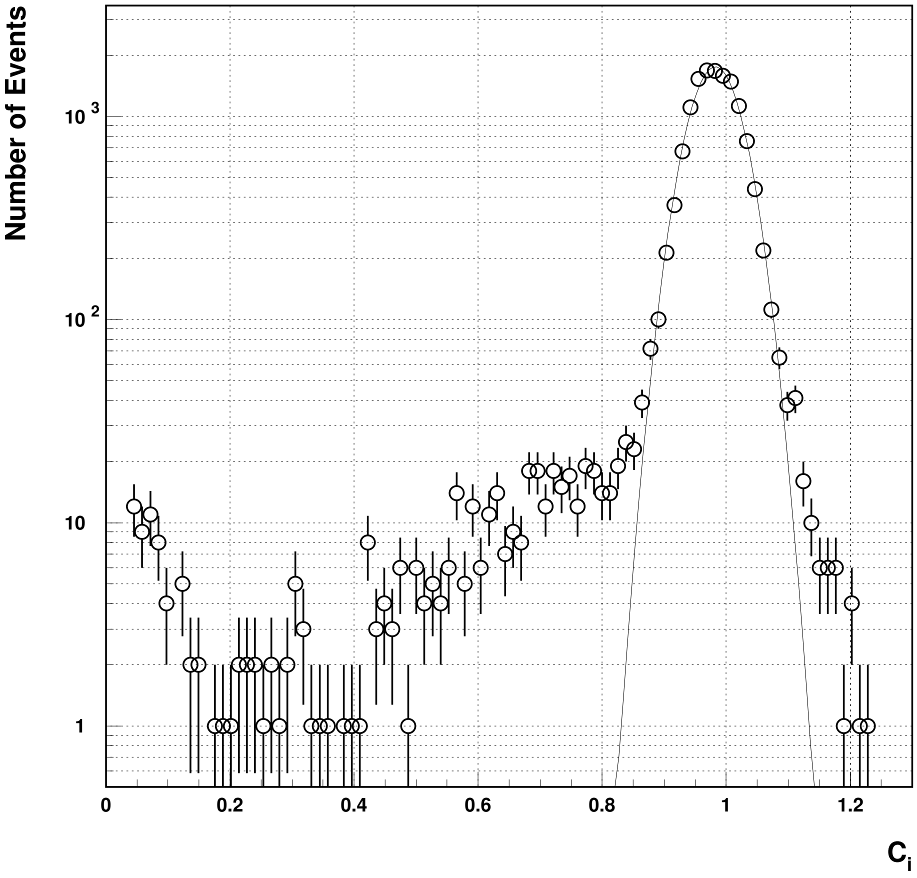

Figure 4: Distribution of the events for $E = 20\ GeV$, $\Theta = 10^o$ as a function of C_i for electrons tagged by Čerenkov counter.

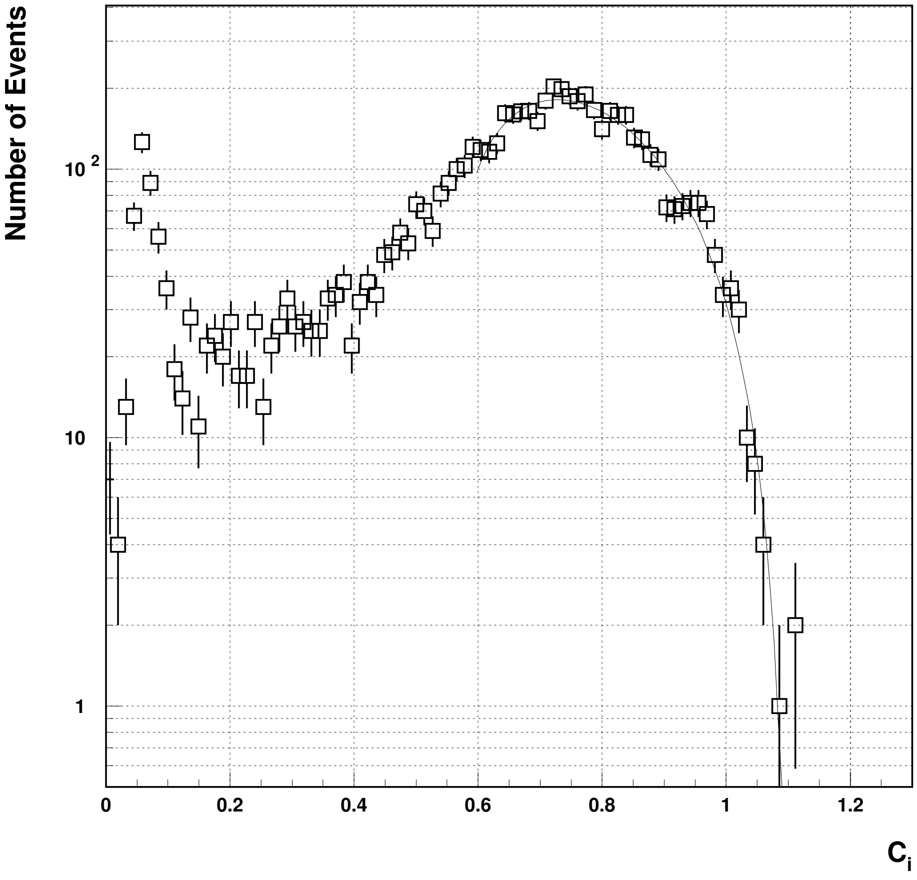

Figure 5: Distribution of the events for $E = 20\ GeV$, $\Theta = 10^o$ as a function of C_i for π- mesons tagged by Čerenkov counter.

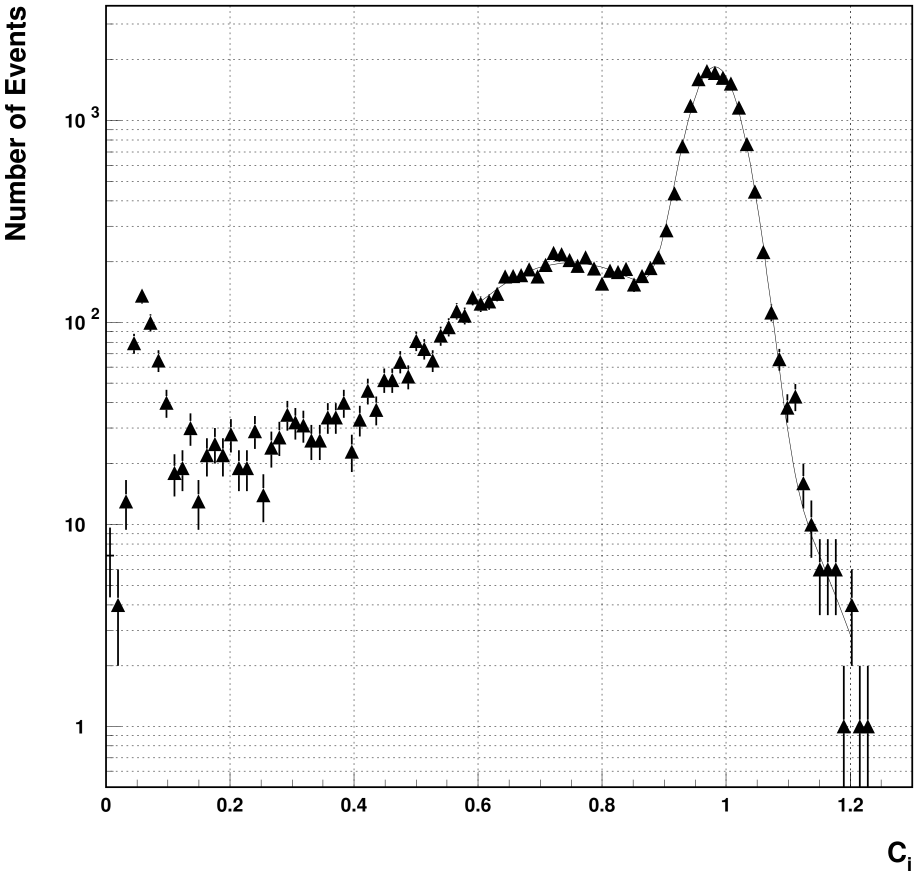

Figure 6: Distribution of the events for $E = 20\ GeV$, $\Theta = 10^o$ as a function of C_i for all events.

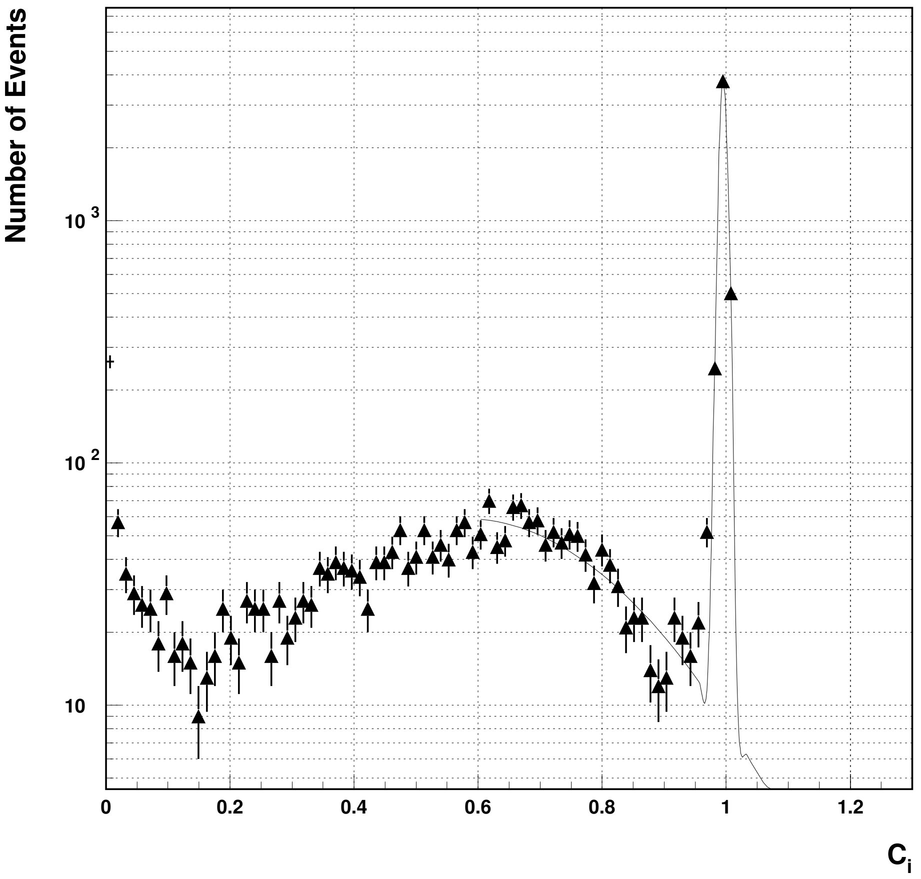

Figure 7: Distribution of the events for $E = 300\ GeV$ electron at $\Theta = 30^o$ as a function of C_i for all events.

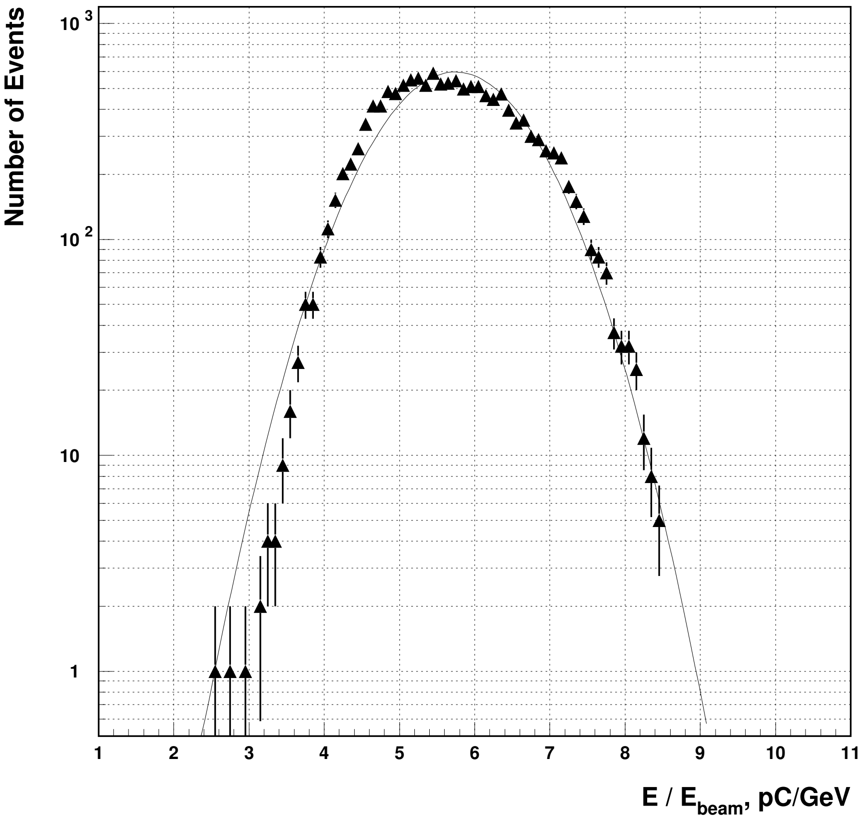

Figure 8: Energy distribution for 20 GeV electrons at 10^o as a function of Z coordinate.

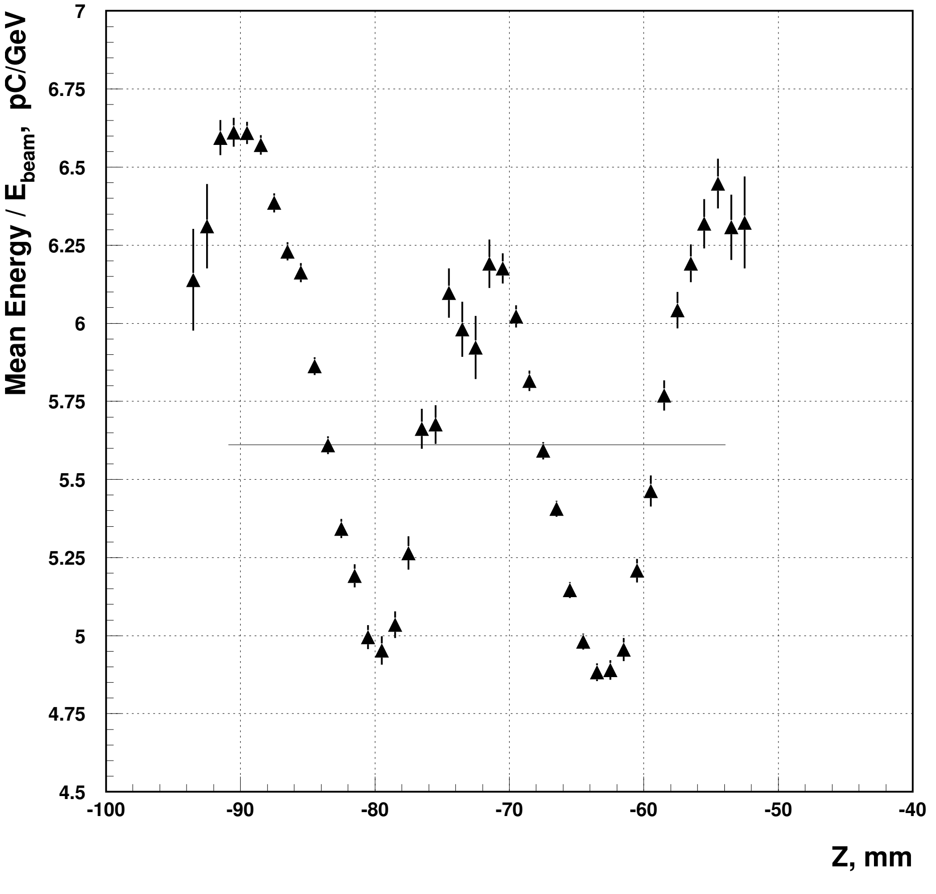

Figure 9: Response to 20 GeV electrons at 10^o as a function of Z coordinate.

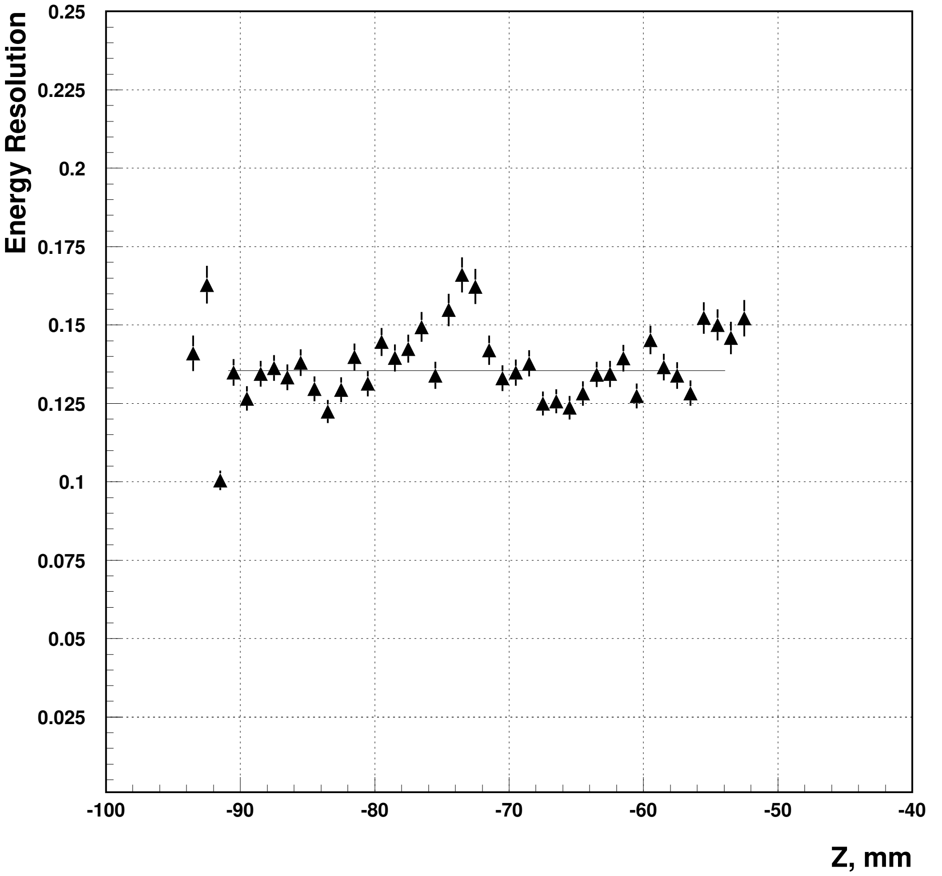

Figure 10: Energy resolution for 20 GeV electrons at 10^o as a function of Z coordinate.

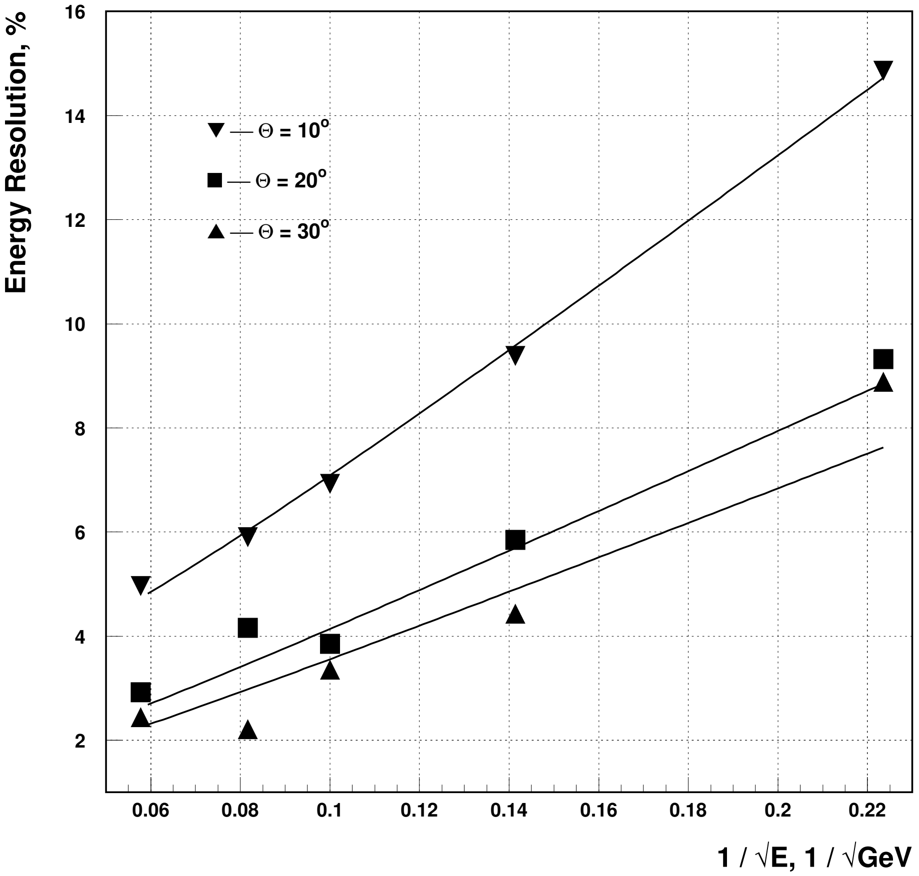

Figure 11: Energy resolution for electrons at 10^o, 20^o and 30^o.

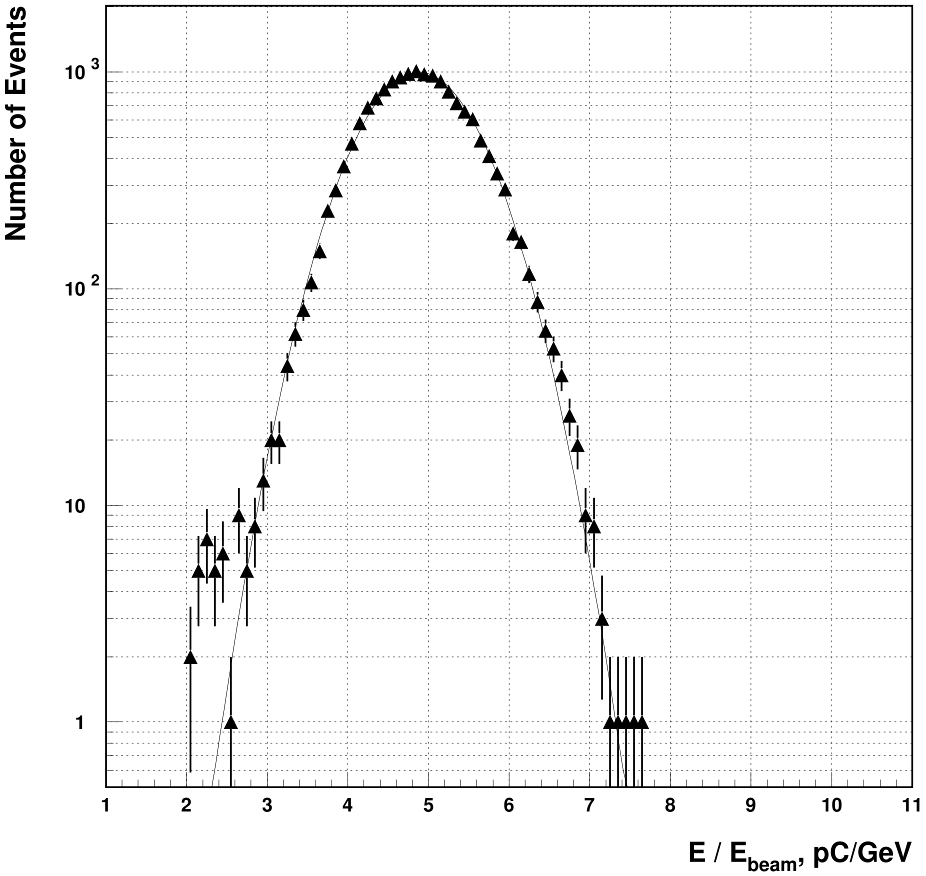

Figure 12: Energy response for 20 *GeV* pions at 20°.

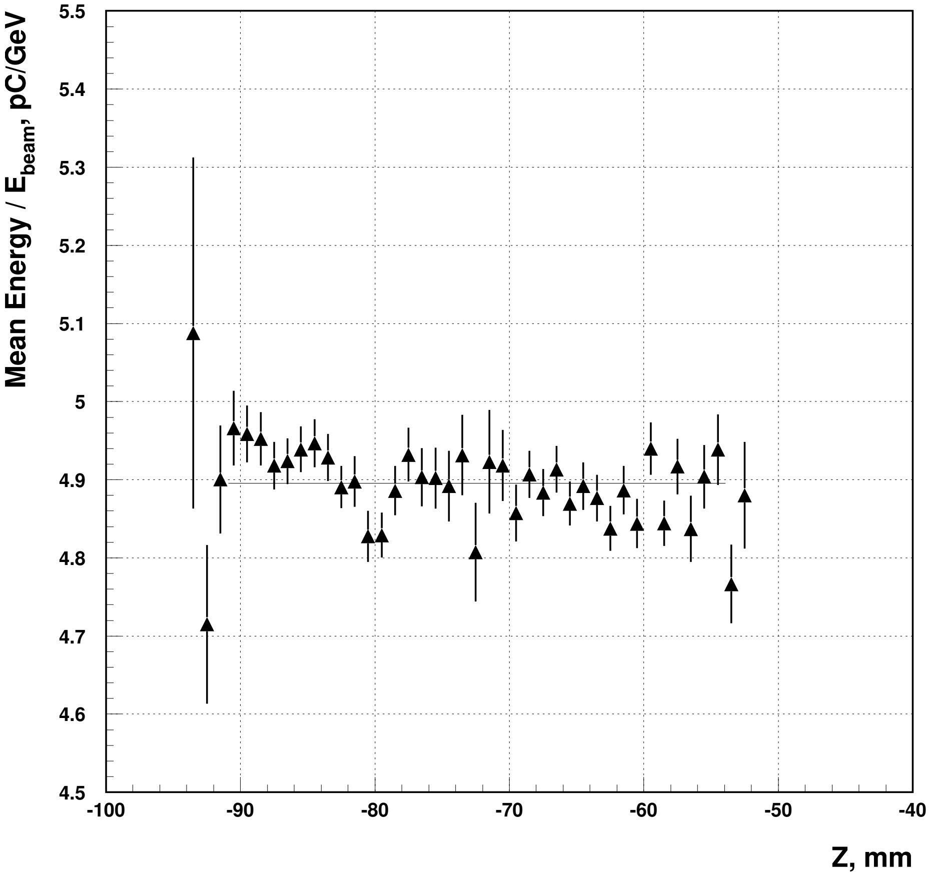

Figure 13: Pion response for 20 *GeV* and 10^o as a function of *Z* coordinate.

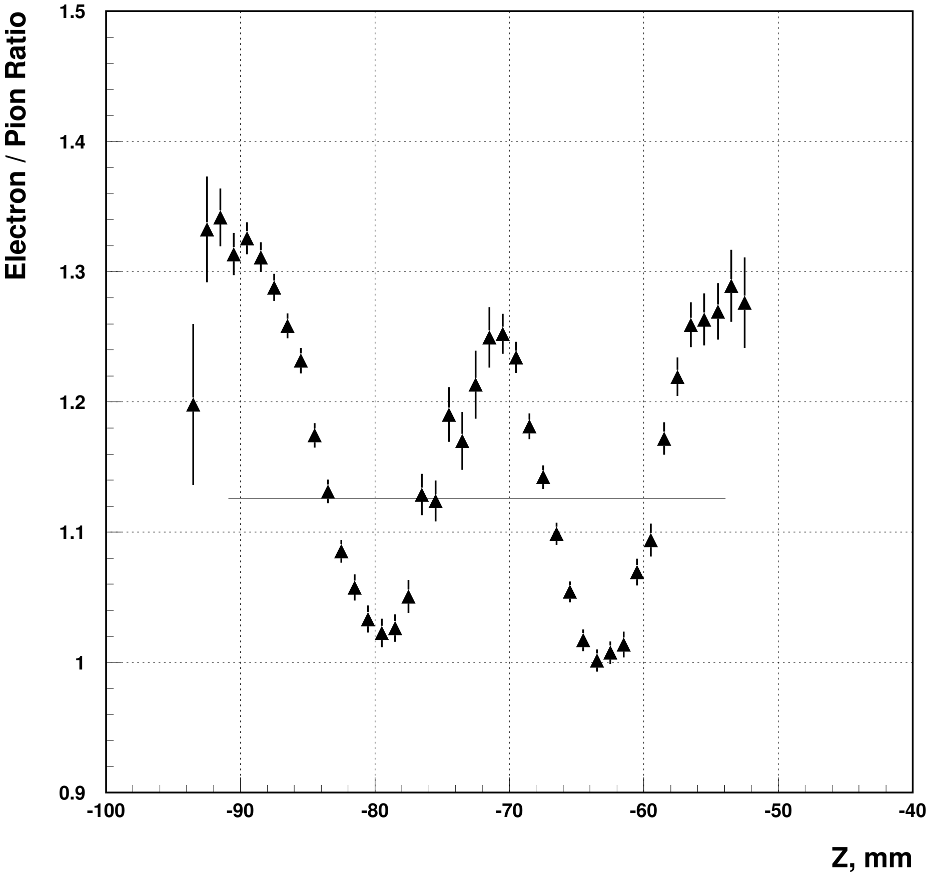

Figure 14: The e/π ratio for 20 GeV at 10^o as a function of Z coordinate.

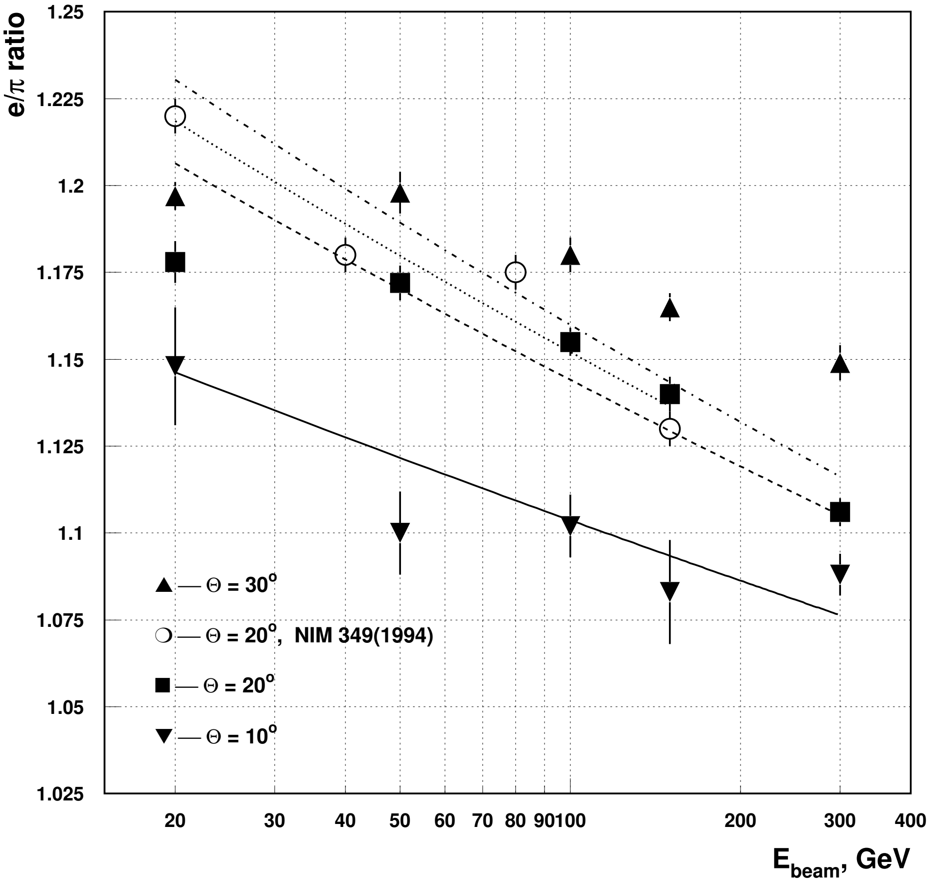

Figure 15: The e/π ratio as a function of energy at 10^o, 20^o and 30^o.

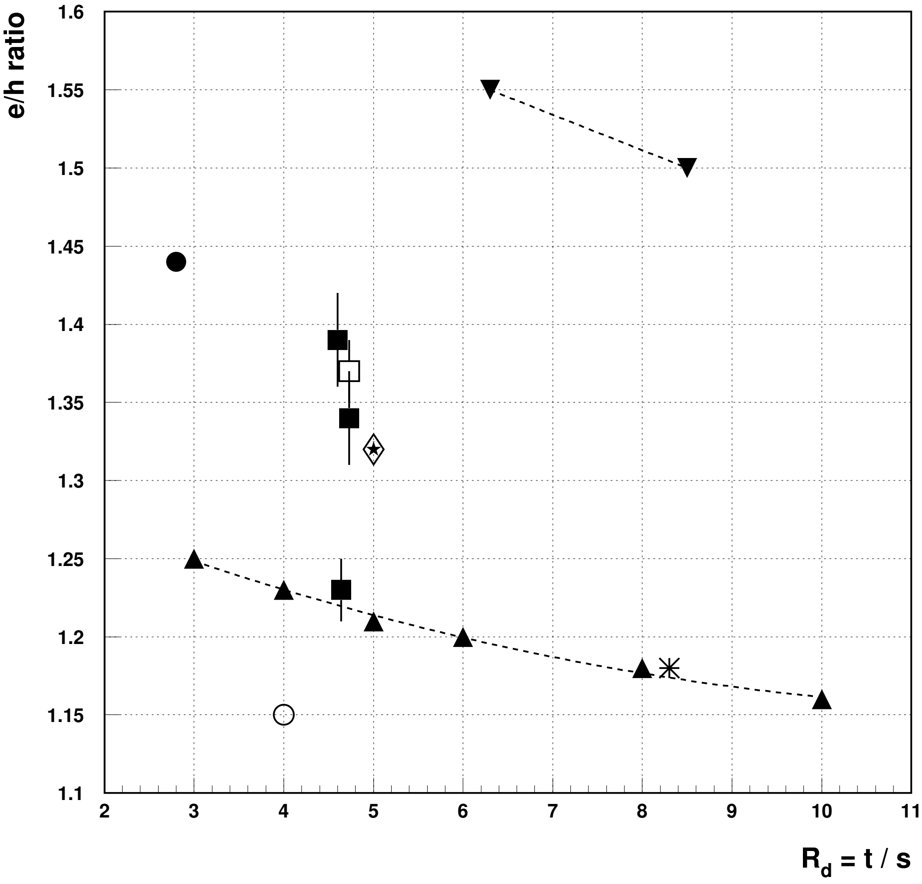

Figure 16: The e/h-ratios as a function of iron and scintillator thicknesses ratio. The lines are the results of fits to some selected data. The meaning of symbols see in Table 9.

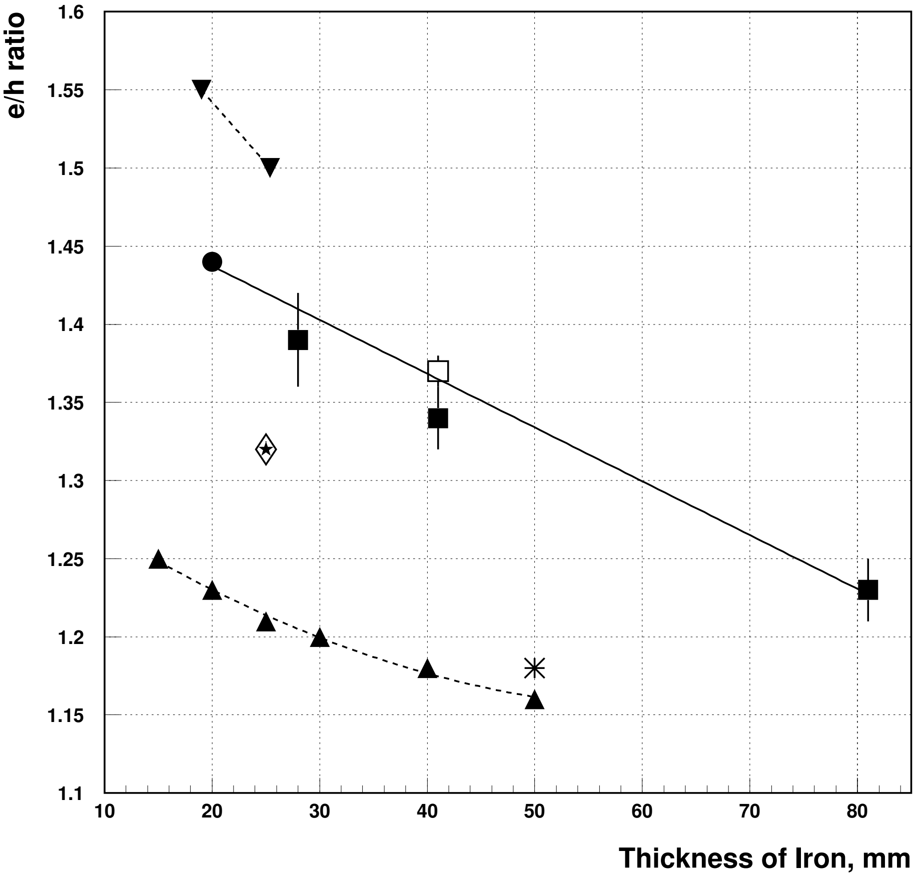

Figure 17: The e/h-ratios as a function of iron thickness. The lines are the results of fits to some selected data. The meaning of symbols see in Table 9.

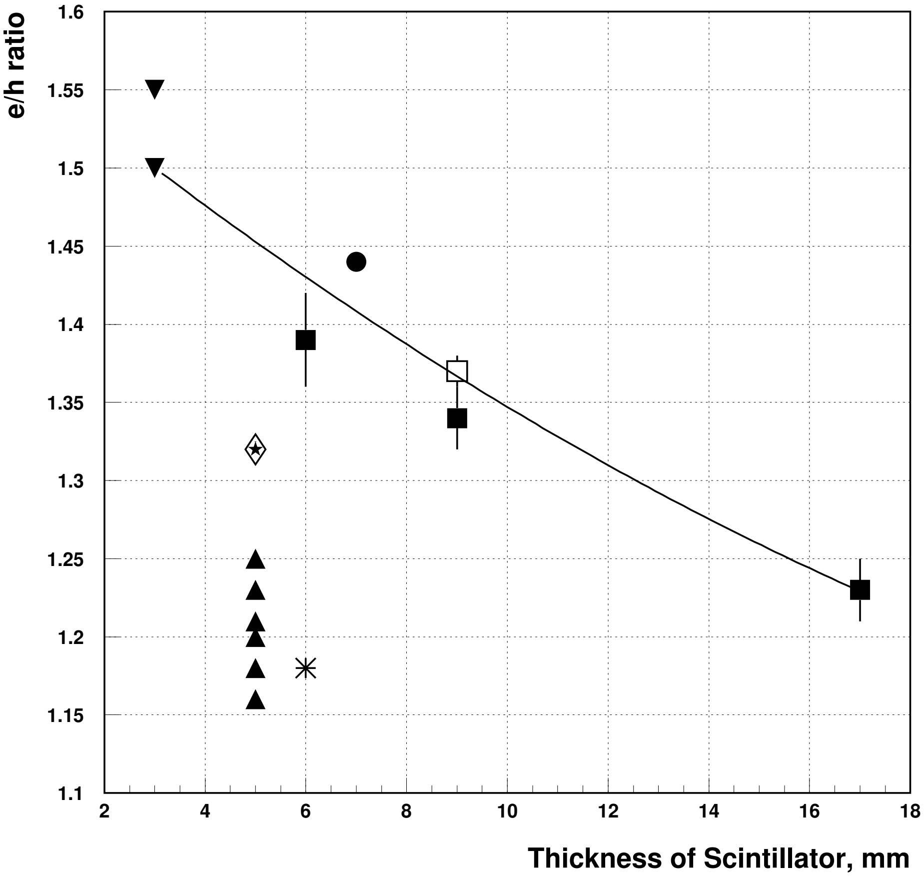

Figure 18: The e/h-ratios as a function of scintillator thickness. The lines is the results of fits to some selected data. The meaning of symbols see in Table 9.